J. Fluid Mech. (2002), *vol.* 461, *pp.* 229–238. © 2002 Cambridge University Press
DOI: 10.1017/S0022112002008662 Printed in the United Kingdom

Nonlinear Smoluchowski slip velocity and micro-vortex generation

By Y. BEN AND H.-C. CHANG

Department of Chemical Engineering, University of Notre Dame, Notre Dame, IN 46556, USA

(Received 28 February 2002 and in revised form 12 March 2002)

When an electric field is applied across a conducting and ion-selective porous granule in an electrolyte solution, a polarized surface layer with excess counter-ions is created. The depth of this layer and the overpotential V across this layer are functions of the normal electric field j on the granule surface. By transforming the ionic flux equations and the Poisson equation into the Painlevé equation of the second type and by analysing the latter's asymptotic solutions, we derive a linear universal j–V correlation at large flux with an electrokinetic slip length β. The flux-induced surface polarization produces a nonlinear Smoluchowski slip velocity that can couple with the granule curvature to produce micro-vortices in micro-devices. Such vortices are impossible in irrotational electrokinetic flow with a constant zeta-potential and a linear slip velocity.

1. Introduction

Electrokinetic flow occurs when an electric field imparts a net electrostatic force in polarized surface regions in an electrolyte to induce solvent flow both within and outside the charged regions. It has been proposed as a convenient means of transporting electrolyte solutions in micro-devices. Since the liquid flow is governed by implantable electrodes, it is far easier to control, direct and meter than the other proposed transportation mechanisms like syringe-displaced, centrifugally driven and Marangoni-driven flows (Stone & Kim 2001). A flat velocity profile also results from electrokinetic flow with the classical linear Smoluchowski slip velocity $u = \epsilon\epsilon_0\zeta E/\eta$, where ϵ and ϵ_0 are the relative and vacuum permittivities, ζ the zeta-potential due to surface charges, η the liquid viscosity and E the tangential electric field. Because the electrostatic body force is confined to a narrow charged Debye layer (10–200 nm) near the surface, it is manifested like a tangential surface force to produce the flat velocity profile. This flat velocity profile is independent of the channel width and minimizes hydrodynamic dispersion (Dutta & Leighton 2001).

However, with low dispersion, electrokinetic flow suffers from mixing deficiencies that reduce reaction yield and promote colloid/protein aggregation/precipitation (Chang 2001; Takhistov, Indeikina & Chang 2002; Minerick, Ostafin & Chang 2002); many of them can be remedied by the generation of micro-vortices within the flow channels. However, generation of micro-vortices is difficult in electrokinetic flow. It was realized long ago (Probstein 1994) that with the linear Smoluchowski slip velocity and uniform ζ-potential, the electrokinetic streamlines are the same as the electric field lines governed by the electric vector field $\boldsymbol{E} = -\nabla\phi$. As a result, both the velocity and electric vector fields are irrotational. Due to the slip condition, viscous electrokinetic flow fields are unique in that they can also be described as

https://doi.org/10.1017/S0022112002008662 Published online by Cambridge University Press

a potential flow at vanishing Reynolds numbers. However, the irrotational feature of potential flow then implies that closed streamlines and vortices are impossible. One can introduce surfaces with non-uniform ζ-potential (Herr *et al.* 2000), but such non-uniformities are difficult to impose at junctions and membrane surfaces where vortex mixing is most needed. Mechanical stirrers of sub-millimetre dimension, like expanding bubbles and pezio-electric actuators, are also not reliable.

There is a unique vortex generation mechanism specific for electrokinetic flows that is promising, first proposed by Dukhin (1991). If a conducting and ion-specific porous granule is inserted into an electrolyte with a uniform electric field, the field lines are attracted to the conducting granule and the counter-ions (assumed to be cations here) carry the flux (current) into the granule but the co-ions do not penetrate into the granule. Since the streamlines do not penetrate the granule, the velocity field no longer coincides with the electric field and is hence no longer irrotational. The finite counter-ion flux requires a linear diffusive concentration gradient in the electro-neutral region near the bulk. With increasing flux j^+, this gradient increases and so does the width of a polarized region near the granule that is depleted of co-ions. This elongation then increases the potential drop V, the overpotential, over the polarized region. If a tangential field E_t is now applied along the granular surface, standard hydrodynamic analysis (Probstein 1994) shows that the slip velocity becomes $u = \epsilon\epsilon_0 V E_t/\eta$, where the overpotential V replaces the ζ-potential and usually exceeds it by several factors. Moreover, since V is a monotonically increasing function of j^+, the counter-ion flux, it is also a monotonically increasing function of the normal current into the granule and hence the normal electric field E_n in the electroneutral Ohmic region away from the polarized region. As a result, $u \sim V(E_n)E_t$ is now a nonlinear Smoluchowski slip velocity. More specifically, consider a granule with a uniform electric field in the plane of the equator (see figure 1): the normal electric field has a minimum at the poles due to the granule curvature and the tangential slip velocity decreases towards them. From continuity, a back pressure must then build up at the poles to eject the fluid radially outwards. A recirculating vortex can then be generated with this nonlinear Smoluchowski slip velocity due to current leakage into the granule. This has been verified in experiments by Mishchuk & Takhistov (1995), reproduced in figure 1 for a 1 mm granule. These vortices last for nearly an hour until the granule is saturated with ions and does not permit additional flux.

However, this vortex generation mechanism has yet to be captured theoretically or numerically. The obstacle is the derivation of the electrostatic slip condition $j^+(V)$ on the granule surface for the Ohmic outer region beyond the diffusion layer. Numerical solutions have been constructed by Rubinstein & Shtilman (1979) and, much earlier, Levich (1962) derived a nonlinear closed-form small-flux condition by expanding about the electroneutral intermediate solution,

$$\frac{j^+ l}{D^+ C_\infty} = 2\left[1 - \exp\left(-\frac{VF}{2RT} + \frac{\ln(p/C_\infty)}{2}\right)\right], \tag{1.1}$$

where l is the diffusion layer thickness, D^+ is the counter-ion diffusivity, C_∞ is the bulk concentration and p is the surface concentration of the counter-ions. Levich's theory predicts that there is a maximum asymptotic current density, the limiting current j^+_{lim} of $(2D^+C_\infty/l)$, at large V. This, however, has been refuted by experimental data and numerical studies that show j^+ can exceed j^+_{lim} by a factor of 2 at large V (Rubinstein & Shtilman 1979). In fact, vortices are expected only when j^+ exceeds j^+_{lim} when the overpotential V is large and sensitive to j^+. Given the surfeit of system parameters, it is also desirable to obtain a closed-form universal condition to simplify the analysis. It

https://doi.org/10.1017/S0022112002008662 Published online by Cambridge University Press

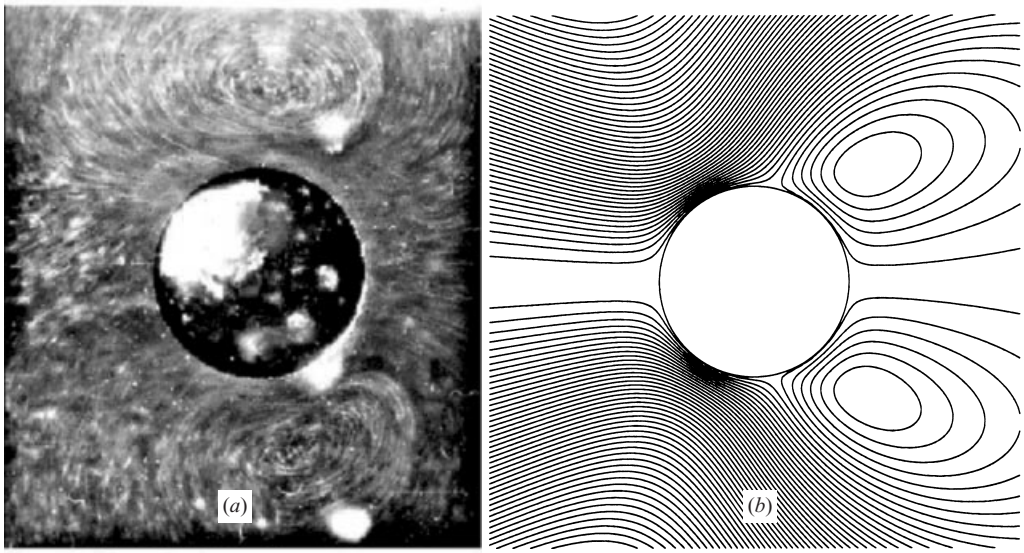


FIGURE 1. (*a*) Illuminated titanium oxide powder shows the streamlines of electrokinetic flow around a 1 mm spherical granule housed in a slot in a field of about $100\,\mathrm{V\,cm^{-1}}$. The electric field is applied towards the left in the plane of the equator and there is significant bulk flow due to the slot zeta-potential. (*b*) Computed streamlines for $R = 1\,\mathrm{mm}$, $E_\infty = 100\,\mathrm{V\,cm^{-1}}$, $C_\infty = 10^{-1}\,\mathrm{mol\,l^{-1}}$, $\lambda = 43\,\mathrm{nm}$, $k = 1$ and $D = 1.994 \times 10^{-5}\,\mathrm{cm^2\,s^{-1}}$. The slight shift of the imaged vortices towards the poles is probably due to the unmodelled flow on the left of the sphere with outward ionic flux.

is even more desirable if the universal electrostatic slip is linear to permit easy solution of the electro-static problem. A universal large-flux electro-static slip condition has not been reported and is an explicitly stated open-problem in Rubinstein (1990). We offer just such a correlation here and use the closed-form solution to confirm Dukhin's vortex formation mechanism. We begin with the problem formulation and a reproduction of earlier numerical results by Rubinstein & Shtilman (1979).

2. Formulation and numerics

The ionic flux is the sum of diffusive flux and electro-migration

$$\boldsymbol{j}^+ = -D^+\nabla C^+ - D^+ z^+ C^+ (F/RT)\nabla\phi, \tag{2.1}$$

where z^+ is the valence of the cation, D^+ its diffusivity, C^+ its concentration and ϕ the electric potential. A similar equation applies for C^- but with a sign change on the electro-migration term. Outside the polarized granule surface, the liquid is well-stirred and the counter- and co-ion concentrations are equal and uniform. This neutral outer Ohmic region then only involves electro-migration and its potential satisfies the Laplace equation $\nabla^2\phi = 0$ obtained by taking the divergence of the flux vector in (2.1) in the absence of concentration gradient.

Hence, the normal ion flux j^+ across the polarized layer is also the normal electric field $\partial\phi/\partial n$ in the Ohmic outer region modulo a factor of $D^+ z^+ C^+ (F/RT)$. The correlation $j^+(V)$ or $j^+(\phi)$ on the surface is then an electro-static slip condition for the Ohmic Laplace equation. The original conducting granule has become one that is between perfectly conducting ($\phi = \mathrm{const}$) or perfectly insulating ($j = 0$) due to the polarization. A desirable linear version of $j^+(V)$ would have the form $\beta' j^+ = (\phi - V_0)$,

https://doi.org/10.1017/S0022112002008662 Published online by Cambridge University Press

or

$$\beta' D^+ z^+ C^+ \left(\frac{F}{RT}\right) \frac{\partial \phi}{\partial n} = (\phi - V_0) \tag{2.2}$$

with $\beta' D^+ z^+ c^+ (F/RT) = \beta$ being the electrostatic slip length. Perfectly conducting and insulating granules then correspond to $\beta = 0$ and ∞, respectively.

We assume that the Ohmic well-stirred region begins at a distance l from the granule surface. Although this diffusion layer thickness depends on the local Péclet number and can vary from one position to another according to its distance from the initiation point of the diffusion layer, we shall assume that it is small compared to the granule size and varies slowly. Hence, at every local position, the dominant variation is in the normal direction and the steady flux equations and the Poisson equation become one-dimensional. With normal electro-migration from the Ohmic region supplying most of the normal current, tangential convection is unimportant except in specifying l. Using l as the characteristic length, $RT/F \sim 24\,\mathrm{mV}$ as the characteristic potential and the bulk concentration C_∞ as the reference concentration, the steady, dimensionless and integrated versions of the flux equation (2.1) for both ions and the Poisson equation become

$$\frac{\mathrm{d}C^+}{\mathrm{d}x} + C^+ \frac{\mathrm{d}\phi}{\mathrm{d}x} = -j, \quad \frac{\mathrm{d}C^-}{\mathrm{d}x} - C^- \frac{\mathrm{d}\phi}{\mathrm{d}x} = 0, \quad \delta^2 \frac{\mathrm{d}^2\phi}{\mathrm{d}x^2} = C^- - C^+, \tag{2.3}$$

where we have omitted the superscript + in j^+ and the small parameter $\delta = \lambda/l$ is the ratio of the Debye length $\lambda = \sqrt{RT\epsilon\epsilon_0/F^2 C_\infty}$ to the diffusion layer thickness l.

Four boundary conditions are required for (2.3) and they are

$$C^+(x=0) = C^-(x=0) = 1, \quad \phi(x=0) = 0, \quad C^+(x=1) = p, \tag{2.4}$$

where x is the inverted and normalized normal coordinate such that $x = 0$ is assigned to the outer boundary that interfaces with the Ohmic outer region. The reference point for the electric potential is also designated there. The granule is then at $x = 1$.

For every given flux j, the solution of (2.3) with boundary conditions (2.4) yields

$$\phi(1) = -V = -V(j, \delta, p). \tag{2.5}$$

This is the inverted form of the electrostatic condition $j(V)$.

Due to the smallness of δ, there exists a neutral intermediate solution away from a small inner region of width δ at $x = 1$. Its solution can be readily constructed from (2.3), with an expansion about the electro-neutral limit at $\delta = 0$,

$$C^+ = C^- = 1 - \tfrac{1}{2} jx; \quad \phi = \ln(1 - \tfrac{1}{2} jx). \tag{2.6}$$

This neutral diffusive intermediate solution has linear concentration profiles and an electric field $\mathrm{d}\phi/\mathrm{d}n$ that increases towards the membrane at $x = 1$. In the limit when $\phi(1) = -V = -\infty$, $j = j_{lim} = 2$. This represents the limiting current due to diffusion limitation for a neutral electrolyte. Without polarization, this is the upper limit of ion flux into the granule.

The inner equation cannot be solved explicitly to allow analytical patching with (2.6). Instead we have numerically integrated (2.3) from $x = 1$ by specifying $\phi(1) = -V$, $(\mathrm{d}\phi/\mathrm{d}x)(1) = -E_1$, $C^+(1) = p$ and $C^-(1) = 0$. The last two conditions are exact and we iterate on the first two until the solutions match (2.6) smoothly at some location x between zero and 1. In figure 2, we depict a standard set of numerical results for this two-parameter iteration scheme. It is clear that the c^+ profile exhibits a minimum in the polarized layer where there is significant ion depletion. In figure 3(a),

https://doi.org/10.1017/S0022112002008662 Published online by Cambridge University Press

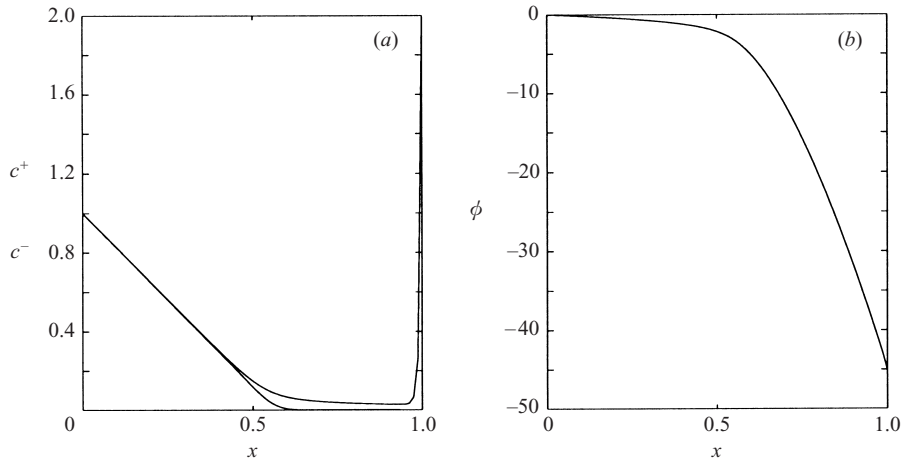


FIGURE 2. The computed profiles of ion concentrations and potential ϕ from numerical matching at $\delta = 0.0127$, $j = 3.5$, $V = 45.18$ and $p = 2.0$, initiated with the intermediate neutral diffusive solution (2.6) on the left near $x = 0$. Deviation from neutrality occurs beyond $x = 0.5$.

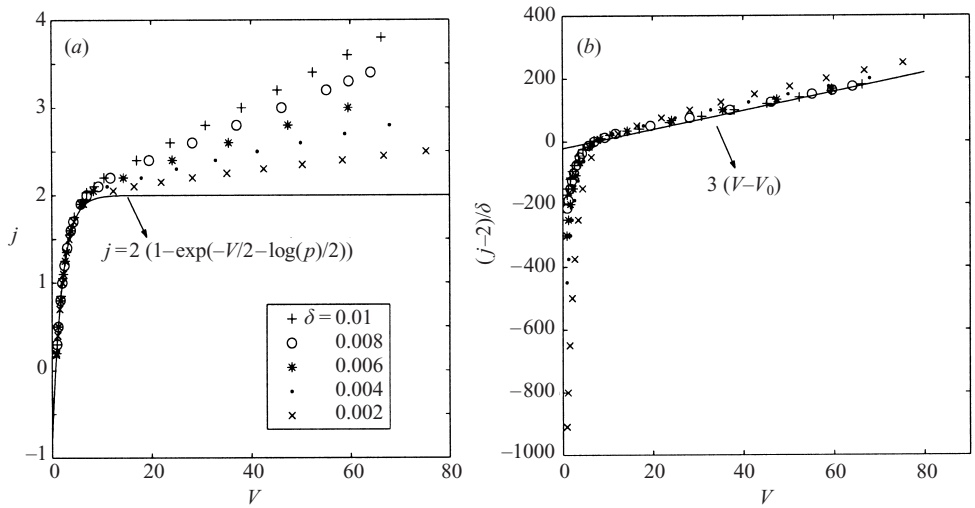


FIGURE 3. (*a*) Raw j–V data from numerical matching for various δ and $p = 2$. Levich's near-equilibrium theory collapses the date for $j < 2$. (*b*) Collapse of large-j data in (*a*) using our theory (3.16).

we depict the computed $j(V)$ correlations. The correlation is clearly highly nonlinear and approaches the result of Levich (1.1) only for $j < j^+_{lim} = 2$. However, the large-flux correlations that show large V sensitivity seem linear although they are quite scattered in the raw coordinates for a wide range of δ and p. They will be collapsed by a universal scaling offered by the matched asymptotics analysis below.

3. Matched asymptotics

Rubinstein (1990) noted that (2.3) can be collapsed into one single nonlinear equation with an ingenious transformation. The ion equations are added together and

https://doi.org/10.1017/S0022112002008662 Published online by Cambridge University Press

the Poisson equation is used to replace the sum of the electro-migration terms

$$\frac{\mathrm{d}}{\mathrm{d}x}(C^+ + C^-) - \delta^2 \frac{\mathrm{d}^2\phi}{\mathrm{d}x^2}\frac{\mathrm{d}\phi}{\mathrm{d}x} = -j. \tag{3.1}$$

Integrating once and recognizing that the no-flux condition on C^- yields a Boltzmann distribution, $C^- = \mathrm{e}^{\phi}$, one obtains

$$C^+ = -jx - \mathrm{e}^{\phi} + \frac{\delta^2}{2}\left(\frac{\mathrm{d}\phi}{\mathrm{d}x}\right)^2 - d, \tag{3.2}$$

where d is an integration constant.

Applying the boundary condition for C^+ at $x = 0$ in (2.4), one specifies the parameter

$$d = -2 + \frac{\delta^2}{2}\left(\frac{\mathrm{d}\phi}{\mathrm{d}x}(0)\right)^2 = -2 + \frac{\delta^2 j^2}{8} \sim -2 \tag{3.3}$$

as $(\mathrm{d}\phi/\mathrm{d}x)(0) = -j/2$ from (2.6) of the electro-neutral solution at $x = 0$. The other boundary condition C^+ at $x = 1$ yields the desired j–V relationship

$$j = -p + 2 - \frac{\delta^2 j^2}{8} - \mathrm{e}^{-V} + \frac{\delta^2}{2}\left[\frac{\mathrm{d}\phi}{\mathrm{d}x}(1)\right]^2. \tag{3.4}$$

Knowledge of $(\mathrm{d}\phi/\mathrm{d}x)(1)$, the field at the granule, would yield the j–V correlation.

Rubinstein (1990) first showed that the transformation

$$\eta = \frac{\exp(\phi/2)}{2^{1/6}(\delta j)^{1/3}}, \quad \xi = \frac{jx - 2 + \delta^2 j^2/8}{2^{1/3}(\delta j)^{2/3}} \tag{3.5}$$

then transforms the Poisson equation, with (3.2) substituted, into the second Painlevé equation (Bender & Orszag 1978)

$$\frac{\mathrm{d}^2\eta}{\mathrm{d}\xi^2} = 2\eta^3 + \xi\eta. \tag{3.6}$$

At $x = 0$ on the outer Ohmic boundary, ξ approaches negative infinity for small δ. Moreover, the neutral diffusive intermediate becomes

$$\eta \sim \sqrt{-\xi/2} \tag{3.7}$$

as $\phi \to 0$ in (3.5) for this limit. The logarithm singularity of (2.6) is removed by (3.5).

At the other boundary on the granule $x = 1$, $\xi_* = (j-2)/(2^{1/3}(\delta j)^{2/3})$ approaches positive infinity for large flux $j > 2$. Moreover, in the limit of $\mathrm{e}^{V/2} \ll \delta^{1/3}$ or $V \gg -\frac{2}{3}\ln\delta$, which is valid for large flux, η vanishes at the granule surface. This means the appropriate trajectory in the (ξ, η)-plane is one that intersects the ξ-axis at ξ_*. Replacing $(\mathrm{d}\phi/\mathrm{d}x)(1)$ by the transformed $(\mathrm{d}\eta/\mathrm{d}\xi)(\xi_*)$ in (3.4), we obtain

$$j = -p + 2 - \mathrm{e}^{-V} - \delta^2 j^2/8 + \frac{2(\delta j)^{4/3}\mathrm{e}^{V}}{2^{1/3}}\left[\frac{\mathrm{d}\eta}{\mathrm{d}\xi}(\xi_*)\right]^2. \tag{3.8}$$

The j–V correlation now reduces to the estimate of $(\mathrm{d}\eta/\mathrm{d}\xi)(\xi_*)$, the slope at the intercept with the ξ-axis of the asymptotic solution of the Painlevé equation at large ξ_*.

This requires an asymptotic expansion of the Painlevé equation in the region near the ξ-axis where $\eta^2 \ll \xi$. In this neighbourhood of the ξ-axis, the first term on the

https://doi.org/10.1017/S0022112002008662 Published online by Cambridge University Press

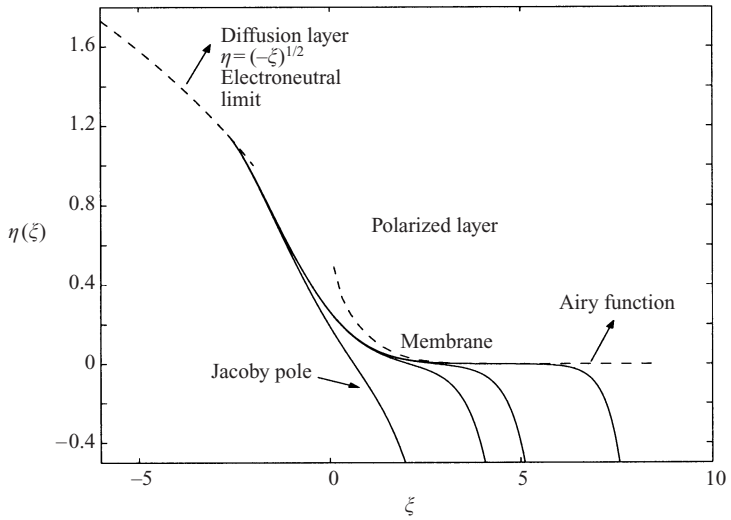


FIGURE 4. Solution trajectories approach the neutral diffusive solution (3.7) at large negative ξ and the Airy function (3.10) at large positive ξ. A movable attracting pole causes each trajectory to approach negative infinity in η at a finite ξ value after the intercept with the ξ-axis.

right-hand side of the Painlevé equation (3.6) is negligible and one obtains the Airy equation

$$\frac{\mathrm{d}^2\eta}{\mathrm{d}\xi^2} = \xi\eta. \tag{3.9}$$

This equation has a unique large-ξ solution, the Airy function (Bender & Orszag 1978),

$$\eta \sim \frac{1}{2\sqrt{\pi}}\xi^{-1/4}\exp(-\tfrac{2}{3}\xi^{3/2}), \tag{3.10}$$

which decays monotonically to zero at large ξ.

We have transformed some of our large-flux numerical solutions to the (ξ,η)-plane in figure 4. It is clear that all trajectories evolve from the neutral diffusive solution to the Airy solution at large flux with an intermediate region that escapes both. However, the blow-up of figure 4 shows that different asymptotic trajectories depart from the Airy function at large ξ and intersect the ξ-axis at different ξ_*. After the intersection at ξ_*, the trajectories approach negative infinity at finite ξ, indicating a movable pole for each trajectory (Bender & Orszag 1978). The different intercepts correspond to different higher-order terms that match (3.7) to (3.10) in the intermediate region. However, the existence of a movable pole means that we can estimate $(\mathrm{d}\eta/\mathrm{d}\xi)(\xi_*)$ without determining these higher-order terms: all intercepts at large ξ have slopes with identical dependence on ξ.

As the trajectory passes the ξ-axis and η blows up in the negative direction at the pole, the condition $\eta^2 \ll \xi$ that leads to the Airy function is no longer valid. Instead, we examine the region when both terms on the right of the Painlevé equation (3.6) are of the same order, $\xi \sim \eta^2$. We hence define new variables $z = \theta/\sqrt{\xi}$ and $t = \xi^{3/2}$ to arrive at the Jacoby equation from an expansion in ξ and t of the Painlevé equation

$$\frac{\mathrm{d}^2 z}{\mathrm{d}t^2} = 2z^3 + z. \tag{3.11}$$

https://doi.org/10.1017/S0022112002008662 Published online by Cambridge University Press

It is well-known that the associated Jacoby elliptic integral yields an infinite number of discrete simple poles t_0, such that $z \sim 1/(t-t_0)$ near the poles. The exact location of the poles is unimportant. We simply need the behaviour of η near its poles ξ_0 from this analysis

$$\eta_{inner} \sim \frac{\sqrt{\xi}}{\xi^{3/2} - \xi_0^{3/2}}. \tag{3.12}$$

Hence, a composite solution of the asymptotic Painlevé trajectory near a particular pole ξ_0 can be constructed from both the Airy function and η_{inner}:

$$\eta_{comp} \sim \frac{1}{2\sqrt{\pi}}\xi^{-1/4}\exp(-\tfrac{2}{3}\xi^{3/2}) + \frac{\sqrt{\xi}}{\xi^{3/2} - \xi_0^{3/2}} \tag{3.13}$$

for large ξ and ξ_0. An expansion of (3.13) for large ξ yields an estimate of the intercept at $\xi_* = (\ln \xi_0)^{2/3}$. Substituting this into (3.13), we conclude that ξ_* is sufficiently smaller than the pole ξ_0 that the inner solution (3.12) does not contribute to the slope at the intercept ξ_*. We can hence use just the slope of the Airy function (3.10) to estimate the slope at the intercept, even though the former does not intersect the ξ-axis,

$$\frac{\mathrm{d}\eta}{\mathrm{d}\xi}(\xi_*) \sim -\frac{\xi_*^{1/4}}{2\sqrt{\pi}}\exp(-\tfrac{2}{3}\xi_*^{3/2}). \tag{3.14}$$

At large ξ_*, the slope of every intercept hence has the same universal dependence on the intercept location ξ_* due to the dominance of the Airy function, which decays monotonically in ξ without singularities.

We can now insert $\xi_* \sim (j-2)/(2^{1/3}(\delta j)^{2/3})$ from (3.5) into (3.14) and substitute the resulting $(\mathrm{d}\eta/\mathrm{d}\xi)(\xi_*)$ into (3.8). Since e^V in (3.8) dominates, we take the logarithm to yield, to leading order,

$$V = \frac{2\sqrt{2}}{3}\left(\frac{j-2}{j^2}\right)^{1/2}\left(\frac{j-2}{\delta}\right) + \ln\frac{(j+p-2)}{0.11\delta j(j-2)}^{1/2}. \tag{3.15}$$

The quantity $(j-2)^{1/2}/j$ approaches a shallow maximum of 0.33 for j beyond 2.5 and remains within 15% of this value for $j < 8$ and similarly for the weak logarithm term, which can be estimated by $V_0(p,\delta) = 1.0 - \ln\delta$ valid for $2 < j < 8$ and $10^{-2} < p < 1$. The p dependence is negligible to leading order. Hence, the electrostatic slip condition at large j can be expressed as a linear condition like (2.2) and as suggested by figure 3(a),

$$(j-2)/\delta = 3.0[V - V_0(\delta)] \tag{3.16}$$

for a large and important region in the parameter space. This version implies that j exceeds the dimensionless limiting current of 2 when V is larger than V_0. Most double layers are 10 to 100 nm while the diffusion layer thickness ranges from 1 to 100 microns. Hence, a typical range of δ is 10^{-4} to 10^{-2}. Using $\delta = 10^{-3}$, we obtain $V_0 \sim 7.9$. Equivalently, the limiting current is exceeded when the overpotential exceeds $7.9(RT/F)$ or about 190 mV. In figure 3(b), we successfully collapse all large-j correlations with (3.16).

A more convenient form of (3.16) for the outer Ohmic region is to determine its limiting electric field at $x = 0$. Relating j to $\mathrm{d}\phi/\mathrm{d}n$ on the Ohmic side, we obtain version (2.2) of the slip condition on the Ohmic side of the surface diffusion layer,

$$\frac{\mathrm{d}\phi}{\mathrm{d}n} = 3.0\delta\phi + 2.0, \tag{3.17}$$

https://doi.org/10.1017/S0022112002008662 Published online by Cambridge University Press

where even V_0 becomes negligible. The dimensionless slip length is then $1/3.0\delta$, corresponding to a dimensional one of $\beta = l/3.0\delta$ in (2.2). This slip length is hence much larger than the diffusion layer thickness and can be as large as 1 mm. The vortices constructed in the next section hence have a characteristic size of one slip length.

4. Vortex generation around a spherical granule

The electrostatic slip length implicit in (2.2) and (3.17) depends on the diffusion layer thickness l, which should grow from the equator towards the poles in figure 1. Moreover, its local thickness is dependent on the local nonlinear slip velocity, which is, in turn, dependent on l. This coupling between electrostatics and hydrodynamics is quite complex. Instead of discussing this coupling in detail, we shall assume a constant diffusion layer here as a simplifying assumption. Using classical diffusion layer scaling for slip boundary conditions, the diffusion layer thickness is $l = kR_0/\sqrt{Pe}$, where $Pe = UR_0/D$, U represents the characteristic velocity of the system to be specified later, R_0 the dimensional particle radius, $D = D^+$, and k is an unknown unit-order coefficient. This completely specifies the effective boundary condition on the ion-specific granule for the electric potential in the well-stirred Ohmic region which obeys the Laplace equation.

Using (3.17) as the boundary condition for the Laplace equation, we obtain from a harmonic expansion the electric potential around a spherical granule in a uniform electric field E_∞

$$\phi = E_\infty \cos\theta \left(r + \left(\frac{1 - 3U\lambda/(k^2 D)}{2 + 3U\lambda/(k^2 D)} \right) \frac{R_0^3}{r^2} \right) - \frac{2k}{3\lambda} \sqrt{\frac{R_0 D}{U}} \frac{RT}{F}. \tag{4.1}$$

The overpotential at the surface and the tangential electric fields are, respectively,

$$\left.\begin{aligned} V = \phi(r = R_0) = E_\infty \cos\theta \left(\frac{3R_0}{2 + 3U\lambda/(k^2 D)} \right) - \frac{2k}{3\lambda} \sqrt{\frac{R_0 D}{U}} \frac{RT}{F}, \\ E_t = -\frac{1}{r} \frac{\partial \phi}{\partial \theta}(r = R_0) = E_\infty \sin\theta \left(\frac{3}{2 + 3U\lambda/(k^2 D)} \right). \end{aligned}\right\} \tag{4.2}$$

Hence, the nonlinear Smoluchowski slip velocity is

$$U_\theta(r = R_0) = \frac{\epsilon\epsilon_0}{\mu} \left(\frac{3E_\infty R_0 \cos\theta}{2 + 3U\lambda/(k^2 D)} - \frac{2k}{3\lambda} \sqrt{\frac{R_0 D}{U}} \frac{RT}{F} \right) E_\infty \sin\theta \left(\frac{3}{2 + 3U\lambda/(k^2 D)} \right) \tag{4.3}$$

and the zero normal liquid flux condition stipulates $U_r(r = a) = 0$. The negative term within the parentheses corresponds to the negative intercept of the j-axis in figure 3 of our large-flux expansion. The true velocity is always positive.

As expected, the polarization ϕ is weakest at the poles ($\theta = \pm\frac{1}{2}\pi$) and largest at the equator ($\theta = 0$) due to E_n variation and the nonlinear Smoluchowski slip velocity, which scales as $\sin\theta\cos\theta$ at large field, has a maximum at $\theta = \frac{1}{4}\pi$. As such, the tangential flow u_θ has a negative downstream gradient $\partial u_\theta/\partial\theta < 0$ for $\frac{1}{4}\pi < \theta < \frac{1}{2}\pi$. By continuity, an outward radial flow must then result from the granule. This, in turn, produces a back-pressure gradient due to flow imbalance away from the granule and drives a vortex.

https://doi.org/10.1017/S0022112002008662 Published online by Cambridge University Press

We now examine the electrokinetic flow field around the sphere. Harmonic expansion of the biharmonic equation for the stream function, with the nonlinear Smoluchowski slip velocity (4.3) and vanishing normal velocity as boundary conditions, yields

$$\psi(r,\theta) = R_0 J\left(r - \frac{R_0^2}{r}\right)\frac{\sin^2\theta}{2} + 2R_0^2 K\left(1 - \frac{R_0^2}{r^2}\right)\frac{\cos\theta\sin^2\theta}{2}, \tag{4.4}$$

where

$$J = -\frac{\epsilon\epsilon_0}{\mu}\frac{2E_\infty}{(2+3U\lambda/(k^2D))}\frac{k}{\lambda}\sqrt{\frac{R_0 D}{U}}\frac{RT}{F} \quad \text{and} \quad K = \frac{9}{2}\frac{\epsilon\epsilon_0}{\mu}\frac{E_\infty^2 R_0}{(2+3U\lambda/(k^2D))^2}.$$

The velocity components in terms of the stream function are: $u_r = (\partial\psi/\partial\theta)/r^2\sin\theta$ and $u_\theta = -(\partial\psi/\partial r)/r\sin\theta$. By averaging the slip velocity (4.3) over $0 < \theta < \frac{1}{2}\pi$ and setting it to U, we can also estimate U and the intensity of the vortices in a self-consistent manner. A constructed flow field which is consistent with the experimental conditions is shown in figure 1. Our derived linear electrostatic slip, (2.2) or (3.17), valid for large-flux $j^+ > j^+_{lim}$ conditions, and the nonlinear slip velocity (4.3) have hence allowed us to verify Dukhin's vortex generation mechanism theoretically.

This work is supported by an NSF-XYZ-on-a-chip grant NSF-CTS99-80745. We are grateful to Pavlo Takhistov for imaging the flow field in figure 1.

REFERENCES

Bender, C. M. & Orszag, S. A. 1978 *Advanced Mathematical Methods for Scientists and Engineering*. McGraw-Hill.

Chang, H.-C. 2001 Bubble/drop transport in microchannels. *The MEMS Handbook*, pp. 11-1–11-3. CRC Press.

Dukhin, S. S. 1991 Electrokinetic phenomena of the second kind and their application. *Adv. Colloid Interface Sci.* **35**, 173–196.

Dutta, D. & Leighton, D. T. 2002 A low dispersion geometry for microchip separation devices. *Anal. Chem.* **74**, 1007–1016.

Herr, A. E., Molho, J. I., Santiago, J. G., Mungal, M. G., Kenny, T. W. & Garguilo, M. G. 2000 Electroosmotic capillary flow with nonuniform zeta potential. *Anal. Chem.* **72**, 1052–1057.

Minerick, A. R., Ostafin, A. E. & Chang, H.-C. 2002 Electrokinetic transport of red blood cells in microcapillaries. *Electrophoresis* (in press).

Levich, V. G. 1962 *Physiochemical Hydrodynamics*. Prentice-Hall.

Mishchuk, N. A. & Takhistov, P. V. 1995 Electroosmosis of the second kind. *Colloids Surf.* A **95**, 119–131.

Probstein, R. F. 1994 *Physiochemical Hydrodynamics*. Wiley-Interscience.

Rubinstein, I. & Shtilman, L. 1979 Voltage against current curves of cation exchange membranes. *J. Chem. Soc. Faraday Trans.* II, **75**, 231–242.

Rubinstein, I. 1990 *Electro-Diffusion of Ions*. SIAM.

Stone, H. A. & Kim, S. 2001 Microfluidics: basic issues, applications, and challenges. *AICHE J.* **47**, 1250–1254.

Takhistov, P., Indeikina, A. & Chang, H.-C. 2002 Electrokinetic displacement of air bubbles in microchannels. *Phys. Fluids* **14**, 1–14.

https://doi.org/10.1017/S0022112002008662 Published online by Cambridge University Press